

Modulating membrane shape and mechanics of minimal cells by light: area increase, softening and interleaflet coupling of membrane models doped with azobenzene-lipid photoswitches

Mina Aleksanyan^{1,2}, Andrea Grafmüller¹, Fucsia Crea³, Vasil N. Georgiev¹, Joachim Heberle³, Rumiana Dimova^{1*}

¹ Max Planck Institute of Colloids and Interfaces, Science Park Golm, 14476 Potsdam, Germany

² Institute for Chemistry and Biochemistry, Free University of Berlin, Berlin, Germany;

³ Department of Physics, Free University of Berlin, Berlin, Germany

* Address for correspondence: Rumiana.Dimova@mpikg.mpg.de

Abstract

Light can effectively interrogate biological systems providing control over complex cellular processes. Particularly advantageous features of photo-induced processes are reversibility, physiological compatibility, and spatiotemporal precision. Understanding the underlying biophysics of light-triggered changes in bio-systems is crucial for cell viability and optimizing clinical applications of photo-induced processes in biotechnology, optogenetics and photopharmacology. Employing membranes doped with the photolipid azobenzene-phosphatidylcholine (azo-PC), we provide a holistic picture of light-triggered changes in membrane morphology, mechanics and dynamics. We combine microscopy of giant vesicles as minimal cell models, Langmuir monolayers, and molecular dynamics simulations. We employ giant vesicle electrodeformation as a facile and accurate approach to quantify the magnitude, reversibility and kinetics of light-induced area expansion/shrinkage as a result of azo-PC photoisomerization and content. Area increase as high as ~25% and a 10-fold decrease in the membrane bending rigidity is observed upon *trans*-to-*cis* azo-PC isomerization. These results are in excellent agreement with simulations data and monolayers. Simulations also show that *trans*-to-*cis* isomerization of azo-PC decreases the membrane leaflet coupling. We demonstrate that light can be used to finely manipulate the shape and mechanics of photolipid-doped minimal cell models and liposomal drug carriers, thus, presenting a promising therapeutic alternative for the repair of cellular disorders.

1. Introduction

Conversion of light into mechanical energy as established with photoresponsive molecules provides a clean and renewable source of energy offering a potential solution to reducing the demand of rapidly-depleting natural resources as well as building a more sustainable world for future generations^[1]. One of the advantageous features of light-induced processes is the high spatiotemporal precision allowing control over the targeted system^[2]. Adjustment of exposure time, intensity, and wavelength of irradiation also reduce the number and amount of byproducts since light-induced processes generally do not require additional reagents^[2b]. Photoprocesses are usually fast and reversible, in which light is used to interconvert photochemically active materials, known as photoswitches, between the low energy, thermodynamically favorable state and high energy, kinetically favorable metastable states^[3].

Among the myriad of photoresponsive molecules in the literature^[4], azobenzene-derived photoswitches are most commonly studied^[5] and the spectrum of applications includes molecular solar thermal energy storage^[1b, 6], catalysis of chemical reactions^[7], generation of photostructured polymers^[8], molecular recognition^[9], modulation of neurotransmission^[10], design of photochromic

materials^[11], drug delivery systems^[12], optoelectronics^[13] and photopharmacological tools^[14]. Typically, azobenzene derivatives isomerize from thermodynamically stable *trans* state to metastable *cis* isomer (π - π^* transition) with the effect of UV-A illumination (365 nm) whereas the irradiation of blue light (465 nm) favors n - π^* transition and reverses the process.^[15] Herein, we employ 1-stearoyl-2-[(E)-4-(4-((4-butylphenyl)diazenyl)phenyl)butanoyl]-sn-glycero-3-phosphocholine photoswitch to build a synthetic photobiomachinery to control membrane shape and mechanics of minimal cells for potential biomedical applications.

In biological cells, it is known that cellular morphology plays an important role in regulating cellular activities such as endocytosis^[16], exocytosis^[17], gene expression mechanisms^[18], stem cell differentiation^[19] and proliferation^[20]. The abnormal changes in the membrane morphology (e.g. excess membrane area with respect to enclosed volume) or the incompetency of biological cells to modulate their membrane mechanics can dramatically affect the cellular homeostasis^[21] and lead to pathological developments^[22], cancer progression^[23] or cell apoptosis^[24]. A fast-responding external trigger such as light for controlling membrane area and mechanics can facilitate transmembrane transport and exchange of substances across the cell membrane thus reducing the above-mentioned harmful effects stemming from the malfunction of cellular processes.

The response of membranes to external triggers can be visualized in giant unilamellar vesicles (GUVs)^[25]. GUVs are occasionally referred to as minimal cells, because of their size and features allowing membrane reconstitution and encapsulation of important cellular elements. Because of their large size, GUVs offer the possibility to directly monitor the membrane under a microscope. Light – triggered changes have been investigated on GUVs to interrogate, among others, (i) light-sensitive proteins embedded in the membrane such as the photoreceptor bacteriorhodopsin^[26], (ii) the photoactivation of channel proteins^[27], (iii) membrane embedded fluorescent dyes which raise the membrane tension and can cause transient poration under irradiation^[28]. The effect of azobenzene derivatives have also been studied with giant vesicles. Examples include light-triggered changes in membrane mechanics^[29] as well as phase state or fluidity^[30]. To the best of our knowledge, the dose-dependent effect of azobenzene derivatives has been explored only to a very limited extent and mainly with water-soluble light switches, which upon insertion into the GUV membrane induce bursting or morphological transformations^[27c, 27d]. Indeed, understanding the fraction-dependent effect of membrane photoswitches is important when considering potential implementation of these molecules for the local modulation of membrane characteristics such as thickness, tension, mechanics and permeability. Water-soluble derivatives are probably less suitable for such application than more hydrophobic membrane analogues.

In this work, we investigate the dose-dependent function of an azobenzene-derived lipid analogue (azobenzene-phosphatidylcholine, azo-PC, see Fig. 1A) applied to the lipid bilayer of giant vesicles to construct artificial photoswitchable cell mimetics from sustainable biomaterials. We subject this system to a thorough investigation for potential biomimetic purposes and applications in biomedical research. In parallel to our minimalistic cell model based on GUVs, we probe the response of Langmuir monolayers with analogous composition and bilayer patches constructed with molecular dynamics (MD) simulations to interrogate the system at leaflet and molecular level, respectively. Characterizations of light-induced membrane shape transformations of GUVs membranes containing azo-PC have been reported previously^[29-30], however, lacking the quantitative link between material properties and membrane parameters such as changes in area and thickness, morphology, and mechanics and their relation to organization and restructuring at the molecular level. Herein, by combining a comprehensive set of experimental methods and model membrane systems with MD simulations, we provide a holistic picture of the photoresponse of membranes containing azo-PC. We first establish an experimentally undemanding approach for direct evaluation of photo-induced area

changes based on GUV deformation in electric fields. The method is then employed to characterize the photoswitch isomerization kinetics and reversibility. Comparison across different model systems is also provided. We elucidate the interrelation between dynamics of photoswitching, membrane mechanics and interleaflet coupling, changes in membrane area and thickness. Finally, we exogenously introduce azo-PC in preformed vesicles and quantitatively monitor the efficiency of photoswitching to test the potential applicability of this photoswitch in cellular studies. Understanding the underlying photoswitching dynamics on the membrane mechanics can elucidate the light-controlled micromanipulation of cellular processes and optimization of light-triggered drug delivery platforms for potential applications of azo-PC containing bio-engineered minimal cells in photopharmacology.

2. Materials and methods

2.1. Vesicle preparation

GUVs were prepared by the electroformation method^[25a] at room temperature (23° C). Varying molar fractions of azo-PC (0, 5, 10, 25, 50, 100 mol %) and 1-palmitoyl-2-oleoyl-sn-glycero-3-phosphocholine (POPC) (both purchased as chloroform solutions from Avanti Polar Lipids, Alabaster, AL) were dissolved in chloroform to a concentration of 4 mM. Then, 8 μ L of this lipid solution was spread as a thin film on a pair of indium-tin oxide (ITO)-coated glass plates (PGO GmbH, Iserlohn, Germany), which are electrically conductive. A stream of N₂ was applied to evaporate most of the chloroform, and the plates were subsequently placed under vacuum for two hours to remove traces of the solvent. For chamber assembly, a Teflon spacer of 2 mm thickness was placed between the ITO-glass plates and the chamber was filled with a solution of 100 mM sucrose (Sigma Aldrich, St. Louis, USA) to hydrate the lipid film. For the GUV electrodeformation studies, the sucrose solution was also supplemented with 0.5 mM NaCl to ensure higher conductivity of the internal solution and thus prolate deformation of the GUVs^[31]. Electrosweeling was initiated by applying a sinusoidal AC electric field at 10 Hz frequency with a 1.6 V (peak to peak) amplitude for 1 hour in the dark. GUVs were then transferred to light-protective glass vials for storage at room temperature and used the same day. For microscopy observations during electrodeformation studies, GUV solutions were diluted 8-fold with 105 mM glucose. The osmolarity was adjusted with an osmometer (Osmomat 3000, Gonotec GmbH, Germany). For bending rigidity measurements, GUV solutions were diluted 1:1 in 85 mM sucrose and 20 mM glucose to avoid gravity effects affecting the fluctuation spectra^[32]. For confocal microscopy observations, GUVs were prepared from 100 mol% azo-PC further doped with 0.1 mol% 1,2-Dioleoyl-sn-glycero-3-phosphoethanolamine labeled with Atto 647N (Atto-647N-DOPE)(Avanti Polar Lipids).

Large unilamellar vesicles (LUVs) were prepared via extrusion at room temperature. Azo-PC (0, 50 and 100 mol %) and POPC (Avanti Polar Lipids, Alabaster, AL) were dissolved in chloroform to a concentration of 10 mg/mL. An aliquot of 100 μ L of the lipid solution was dried under a gentle stream of nitrogen until the formation of a film on the walls of a glass vial. The vial was placed in a desiccator under vacuum overnight for the complete evaporation of the chloroform. The dried lipid film was hydrated with 1 mL Milli-Q water and agitated with a vortex mixer. The suspension was extruded 31 times through a polycarbonate membrane (Whatman® Nuclepore™ Track-Etched Membranes, Merck, Germany) with pore size of 200 nm using a mini-extruder (Avanti Polar Lipids).

2.2. Preparation of Langmuir monolayers and area change measurements in a Langmuir-Blodgett trough

Azo-PC and POPC lipids were diluted to 1 mg/mL in chloroform. The two solutions were mixed in the desired ratios: 0 %, 10 %, 25 %, 50 %, and 100 % azo-PC molar fraction in POPC. An aliquot of lipid chloroform solution was deposited on the water surface of a commercial Langmuir-Blodgett trough (Kibron MicroTroughX, Kibron, Finland) with an available surface of 80 × 350 mm², in the correct amount (about 16 μ L) to yield an initial lipid density at the air-water interface of 100 Å²/lipid. A UV rod lamp (365 nm, Camag, Switzerland) and an array of blue LEDs (450 nm, Luxeonstar, Canada) placed

above the film illuminated the trough surface with a power density of 30 $\mu\text{W}/\text{cm}^2$ and 10 mW/cm^2 , respectively. The power density was measured at the sample position with a handheld power meter (LaserCheck, Coherent, USA). The film was first illuminated for 10 minutes with blue or UV light, respectively, to obtain either the *trans* or the *cis* isomer of the azo-PC component of the deposited lipids, and then compressed to a lateral pressure of 30 mN/m reducing the available area by compression with Teflon barriers at a speed of 35 mm/min .

Compression isotherms during illuminations with both light sources and for all azo-PC molar fractions, were recorded with a sampling rate of 0.25 s^{-1} . To calculate the area expansion as a percentage of the footprint of azo-PC in the *trans* state, the area per lipid at 30 mN/m occupied under blue-light illumination (azo-PC in the *trans* state) was subtracted by the value obtained under UV light illumination (azo-PC in the *cis* state) and divided by the first value. A subsequent new *trans* isotherm was recorded to then calculate the area reduction in analogy. For each azo-PC fraction, the results from four or five illumination cycles on different films were calculated.

2.3. Vesicle electrodeformation and area change measurements

Electrodeformation experiments to measure vesicle area changes^[33] were conducted in a commercial Eppendorf electrofusion chamber (Eppendorf, Germany) described previously. The chamber has two parallel cylindrical platinum electrodes (92 μm in radius) spaced 500 μm apart. GUVs between the electrodes were exposed to a sinusoidal AC field at 1 MHz with a 5 V (peak to peak) amplitude. In the absence of an electric field, the vesicles are quasi-spherical and exhibit visual fluctuations. The membrane area stored in these fluctuations is not possible to assess directly from the microscopy images. The mild AC-field deforms the GUVs and the type of the deformation depends on the field frequency and conductivity ratio between the internal and external GUV solutions^[34]. At the conditions employed here, the GUVs adopt prolate ellipsoidal shapes, allowing for the precise measure of the total vesicle area from the vesicle geometry:

$$A = 2\pi b \left(b + a \frac{\sin^{-1} \epsilon}{\epsilon} \right) \quad (1)$$

where a and b are the vesicle semi-axes along and perpendicular to the applied electric field, respectively, and ϵ is the ellipticity defined as $\epsilon^2 = 1 - (b/a)^2$. Subsequently, the GUVs were irradiated with UV and blue light while the AC-field was still on and the vesicles recorded for 25-30 seconds at an acquisition speed of 8 frames per second (fps). Subtracting the initial vesicle area in the absence of irradiation (but with applied field), A_i , from the vesicle area when exposed to light with specific wavelength, A_l , yields the percentage of relative area increase as $\frac{A_l - A_i}{A_i} \times 100\%$ associated only with the photoisomerization of the azo-PC molecules.

The length of the semi-axes was measured from the recorded vesicle images either manually or using a home-developed software for GUV contour detection^[35]. Data and statistics for GUVs with varying azo-PC fractions were plotted and analyzed using Origin Pro software. At least 10 GUVs from 3 separate sets of experiments for each investigated azo-PC fraction were used to plot the graphs. The statistical significance of the vesicle area changes due to photoswitching was tested with the one-way analysis of variance (ANOVA).

2.4. Vesicle imaging and irradiation

UV-induced shape transformations of 100 mol% azo-PC GUV was monitored through Leica TCS SP8 scanning confocal microscope (Wetzlar, Germany) using a HC PL FLUOTAR 40 \times / Numerical Aperture (NA) 0.6 (air) objective. The pinhole size during the experiment was set to 1 AU (Airy units) and the scanning speed was 400 Hz in unidirectional mode. The Atto-647N-DOPE dye was excited with a HeNe 633 nm laser with 3 % (laser intensity) and the emission signal was collected with a HyD (hybrid)

detector in the range 645–705 nm. In order to observe photoisomerization response of GUVs, external 365 nm UV-LED (maximum power intensity of 20 mW cm⁻², Roschwege, Germany) was attached to the condenser of the confocal microscope. The observation chamber was made of two cover slips (22 x 40 mm and 22 x 22 mm, Knittel Glass, Germany) sandwiching a spacer with a thickness of 1 mm.

Electrodeformation measurements were performed under phase contrast mode of an inverted microscope Axio Observer D1 (Zeiss, Germany), equipped with a Ph2 20× (NA 0.4) objective. Images were taken with an ORCA R2 CCD camera (Hamamatsu, Japan); see also section 2.5 for the setup used for bending rigidity measurements. The GUVs were placed in an Eppendorf electrofusion chamber with approximate thickness of 8 mm (other specifications are indicated in section 2.3). For UV and blue irradiation of the samples, the light from the microscope mercury lamp (HBO 100W) mounted in epi-illumination mode passed through 365 and 470/40 nm filters, respectively. The irradiation power of the HBO lamp was 60 mW cm⁻² for the UV filter set (365 nm) and 26 mW cm⁻² for the blue filter. Power intensities were measured with LaserCheck power meter after the objective and at the position of the sample.

2.5. Bending rigidity measurements

The membrane bending rigidity was measured with fluctuation spectroscopy of the thermal undulations of quasi-spherical vesicles as reported previously^[32, 35]. Membrane fluctuations were observed under phase contrast of an inverted microscope Axio Observer D1 (Zeiss, Germany) equipped with a PH2 40 x (0.6 NA) objective. Sequences of 3000 images each we recorded with Pco.Edge sCMOS camera (PCO AG, Kelheim, Germany) at an acquisition rate of 25 fps and exposure time of 200 μs (the same camera was used also for imaging kinetics of vesicle deformation under photoisomerization imaged at 100 fps). The vesicle contour was detected and analyzed with a home-developed software^[35]. Low crossover modes were selected as 3 – 5 for eliminating the effects of vesicle tensions. Only defect-free, quasi-spherical vesicles with low tension values in the range 10⁻⁷– 10⁻⁹ N m⁻¹ and 10 – 25 μm in radius were analyzed.

2.6. MD simulations

POPC lipids were modeled using the amber Lipid14 force field^[36]; parameters for the azo tail of azo-PC were taken from the optimized parameters for azobenzene from ref.^[37] based on the general AMBER force field^[38]. Figure 1B shows the simulated structures of azo-PC and the respective conformations under UV and blue light. The partial charges for the tails were derived following the methodology used in the Lipid14 force field^[36] using 50 conformations from a 50 ns MD trajectory and the R.E.D. tool scripts^[39]. The topologies for azo-PC and POPC lipids were converted using the glycam2gmx.pl script^[40].

The initial topology of the POPC bilayer structure with 400 lipids was generated using the CHARMM-GUI^[41] and charmm lipid2amber.py script^[42]; coordinates for the azo-PC bilayers were created from the POPC bilayer by fitting and replacing the required number of oleoyl tails with azo tails using VMD^[43]. The bilayer systems were then solvated with 24467 TIP3P water molecules^[44].

All simulations were performed using GROMACS version 5.1.2^[45]. Systems were energy minimized with steepest descend and equilibrated with and without position restraints on the lipids for a total of 21 ns using the weak coupling scheme^[46] to relax the size of the simulation box. Production runs were performed for 100 ns at 303 K, applying the Nose-Hoover thermostat^[47] and Parrinello-Rahman barostat^[48] to keep the pressure and temperature constant.

The bilayer thickness was defined from the distance between the maxima in the phosphate atom distribution along the bilayer normal. Bilayer elastic properties were calculated as follows: The bilayer stretching modulus K_A was obtained from simulations of all bilayer compositions at lateral pressures

of -2, -4, -8, -12 and -16 bar. K_A is found from a linear fit of $\Sigma(A) = K_A \frac{A^{lip} - A_0^{lip}}{A_0^{lip}}$, where Σ is the mechanical tension, A^{lip} the area per lipid and A_0^{lip} the area per lipid of a bilayer with zero mechanical tension. The bending modulus κ was calculated from the lipid splay distribution as described in Ref. ^[49] using the python modules available at https://github.com/njohner/ost_pymodules/^[50].

2.7. LUV area change measurements via dynamic light scattering (DLS)

The average diameter of the LUVs was measured through Zetasizer Nano ZS90 DLS (Malvern Instruments, Malvern, United Kingdom) equipped with a 632.8nm 4mW HeNe laser and measuring the scattered light at 173°. In order to detect the UV-induced area change of the LUVs, the UV LED (used also for the measurements with GUVs) was mounted inside the measuring compartment of the Zetasizer. Three replicates were produced for each light condition for each sample. The average size distribution of the LUVs was plotted and the area of LUVs was calculated from the formula of a sphere, $4\pi R^2$, in which R is the LUV radius. Area increase is defined as for the GUV measurements, namely as $\frac{A_L - A_i}{A_i} \times 100$ where A_L is the vesicle area after the UV exposure and A_i is the initial area of the vesicle before the UV irradiation.

2.8. Exogenous addition of azo-PC

For exposing preformed GUVs to exogenous azo-PC, pure POPC GUVs prepared in 100 mM sucrose solution were diluted 1:1 in 105 mM glucose solution to a final volume of 174 μ L, which was then mixed with 1 μ L of 2.72 mM azo-PC dissolved in 2:1 (vol) dichloromethane/methanol solution. The final concentration of azo-PC in the GUV suspension was 15.56 μ M being close to the total amount of POPC lipids forming the vesicles, i.e. the final azo-PC-to-POPC ratio was about 1:1. After 20 minutes of incubation allowing the evaporation of the organic solvents, POPC GUVs enriched with azo-PC were placed in an observation chamber and exposed to UV and blue irradiation, respectively, and monitored by phase-contrast imaging.

3. Results and discussion

3.1. Vesicle shape deformation under light

Previously, pure azo-PC GUVs have been explored under dark-field and epifluorescence microscopy, to detect effects of illumination ^[29-30]. These approaches require respectively intense white light illumination and a substantial fraction of a membrane fluorophore. Here, we implemented confocal microscopy, which offers higher resolution of the photo-induced membrane deformations and, compared to epifluorescence observations, requires only one-tenth of the fraction of the membrane fluorophore (0.1 mol%) for visualization. It is noted that high fractions of fluorophores affect membrane material properties such as bending rigidity^[51] and can cause oxidation and changes in membrane composition^[52]. In addition, we probed the response of vesicles devoid of fluorescent dye using phase-contrast microscopy to eliminate potential dye effects. The UV irradiation in our confocal setup was implemented with an external source mounted at the microscope condenser, see Methods section 2.4. GUVs containing azo-PC and labeled with 0.1 mol % Atto-647N-DOPE were exposed to UV light to initiate *trans*-to-*cis* photoisomerization and observed for a few seconds. Before UV irradiation, GUVs were mostly defect free (at least 90 % of the population) exhibiting thermal fluctuations visible both in confocal and phase-contrast microscopy. Upon UV illumination, GUVs containing substantial fractions of azo-PC (50 or 100 mol%) undergo large shape transformations including complex budding events within a few seconds visible in confocal and phase contrast microscopy (Figs. 1C,D, S1 and Movies S1, S2 and S3). The vesicles increase in size (see last snapshot in Fig. 1D), but a quantitative assessment of the membrane area change is not feasible because of the unknown GUV geometry as

even if the vesicle appears as a sphere in the projected image, it can be flattened due to gravity into an oblate shape which has similar appearance in the images.

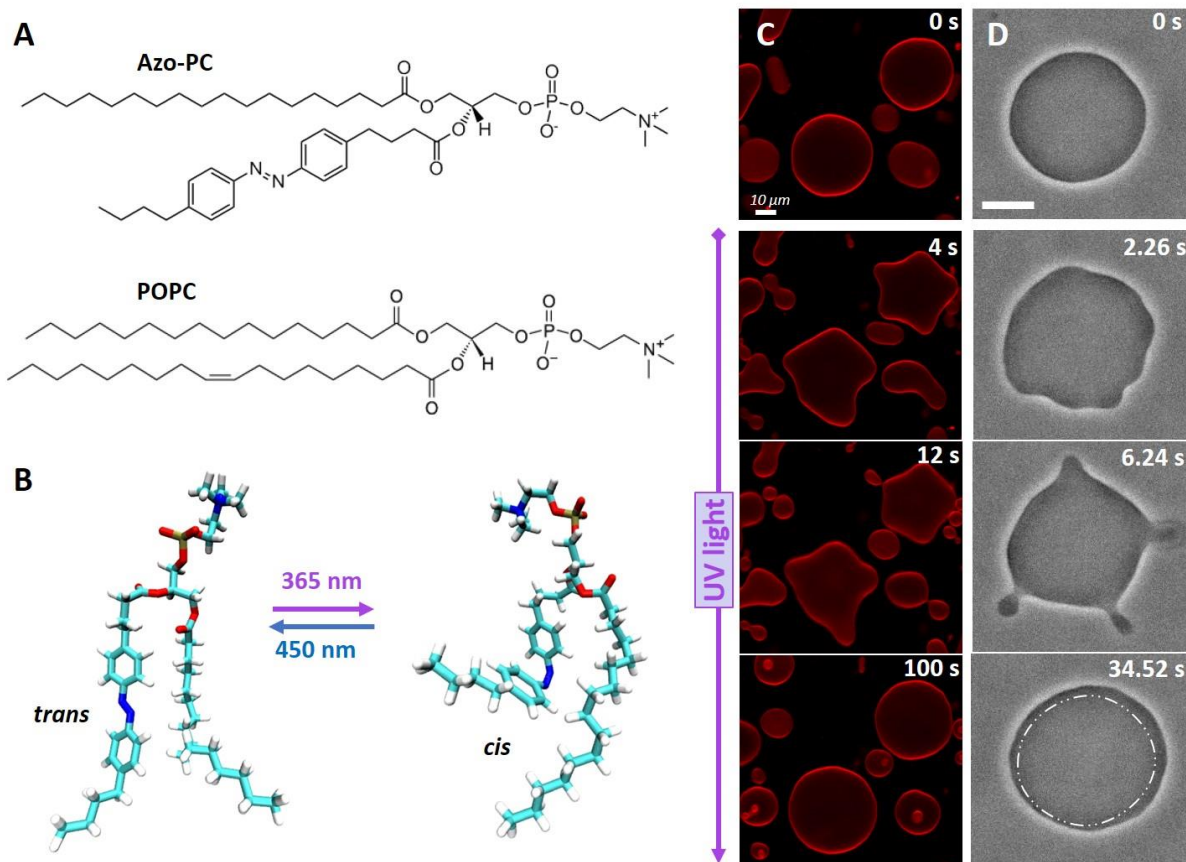


Figure 1: *Trans-to-cis* photoisomerization of azo-PC triggers vesicle shape changes and area increase. (A) Chemical structures of azo-PC and the POPC. (B) Representative snapshots of the molecular conformational changes upon photo isomerization of azo-PC obtained from MD simulations. (C) Confocal cross section images of 100 mol% azo-PC GUVs labelled with 0.1 mol% Atto-647N-DOPE monitored during photoisomerization. Upon UV irradiation (365 nm), the GUVs undergo complex shape transformations of outward budding and bud re-adsorption over time; the time stamps are shown in the upper part of the images. (D) Phase contrast microscopy showing a time sequence of the *trans-to-cis* photoisomerization response of 50 mol % azo-PC doped vesicles (azo-PC:POPC 50:50) under UV illumination, see also Movie S2. Budding and bud re-adsorption occur over time. The area of the vesicle increases: for comparison, the dash-dotted contour in the last image shows the approximate GUV contour before irradiation (first snapshot). Scale bars correspond to 10 μm .

3.2. Assessing the light-induced membrane area change by GUVs electrodeformation, Langmuir monolayer isotherms, and MD simulations

To quantitatively characterize the membrane area change associated with photoisomerization, we employed GUV electrodeformation^[33a, 34b]. In this approach, an alternating current (AC) field is applied before exposing GUVs to the UV light. Moderate strengths of electric fields are able to pull the excess area stored in thermal fluctuations. The vesicles deform into prolate or oblate shapes depending on the AC field frequency and conductivity ratio between the internal and external GUV solutions^[31, 34b]. Due to gravity, oblate vesicles lie flat in the observation chamber and appear as spherical in the projected images not allowing access to their short semi-axis. On the contrary, prolate deformations, whereby the vesicle elongates along the field direction parallel to the bottom of the observation chamber, allow measuring both semi-axes a and b (Fig. 2A), and thus, the correct evaluation of the vesicle area. To induce prolate deformation, we prepared the GUVs in solutions containing salt (0.5

mM NaCl and 100 mM sucrose) and diluted the harvested vesicles in salt-free glucose solution (105mM). These conditions ensure higher conductivity in the GUV interior rendering them prolate under the applied AC field. Additionally, due to the refractive index differences between the interior and exterior sugar solutions, the GUVs appeared with a sharp contour under phase contrast observations (Fig. 1D) facilitating image analysis and area measurements.

We explored the area change in POPC vesicles containing 0, 5, 10, 25, 50 and 100 mol% azo-PC. The vesicles were first exposed to an AC field and the area was measured. Then, while keeping the AC field on, they were irradiated with UV light and the changes in vesicle shape were characterized in terms of changes in the vesicle aspect ratio a/b . The morphology change of each GUV was monitored over time under phase-contrast microscopy during the application of electric field and UV-light (see Fig. 2A-C, Fig. S2 and Movies S4-S6). The vesicle response to AC field is fast and completes within less than a second (the dynamics practically depends on the field strength and membrane viscosity^[53]). The degree of deformation of the vesicles in the AC field in the absence of UV light showed variations from vesicle to vesicle. These are imposed by the vesicle size (affecting the magnitude of the Maxwell stress tensor deforming the vesicle) and the initial available excess area for deformation (which cannot be controlled as the GUV preparation method yields vesicles with different tensions).

UV illumination was typically applied ~10 seconds after applying the AC field. Pure POPC GUVs did not show any response to UV light, see gray trace in Fig. 2B and Movie S4. The response of azo-PC-doped GUVs to UV light was very fast. GUVs containing 5, 10 and 25 mol% azo-PC reached their maximum deformation within a second after switching the UV light on (Figs. 2B, S2A and Movie S5). Increasing fractions of azo-PC resulted in larger membrane deformations in the form of buds (a couple of micrometers in size, see zoomed image in Fig. 2C) requiring longer times for the created membrane area to be pulled out into ellipsoidal shape. For GUVs with 50 mol% azo-PC, the buds pulled back by the electric field within roughly 12 – 15 seconds after applying the UV light, contributing to the vesicle elongation. These results indicate that budding and bud re-adsorption slowed down the deformation processes of GUVs containing high fractions of azo-PC (50 mol% and more), see Figs. 2C, S2B and Movie S6). Indeed, vesicles made of 100 mol% azo-PC often did not reach perfect elliptical shapes affecting our accuracy for assessing the membrane area increase.

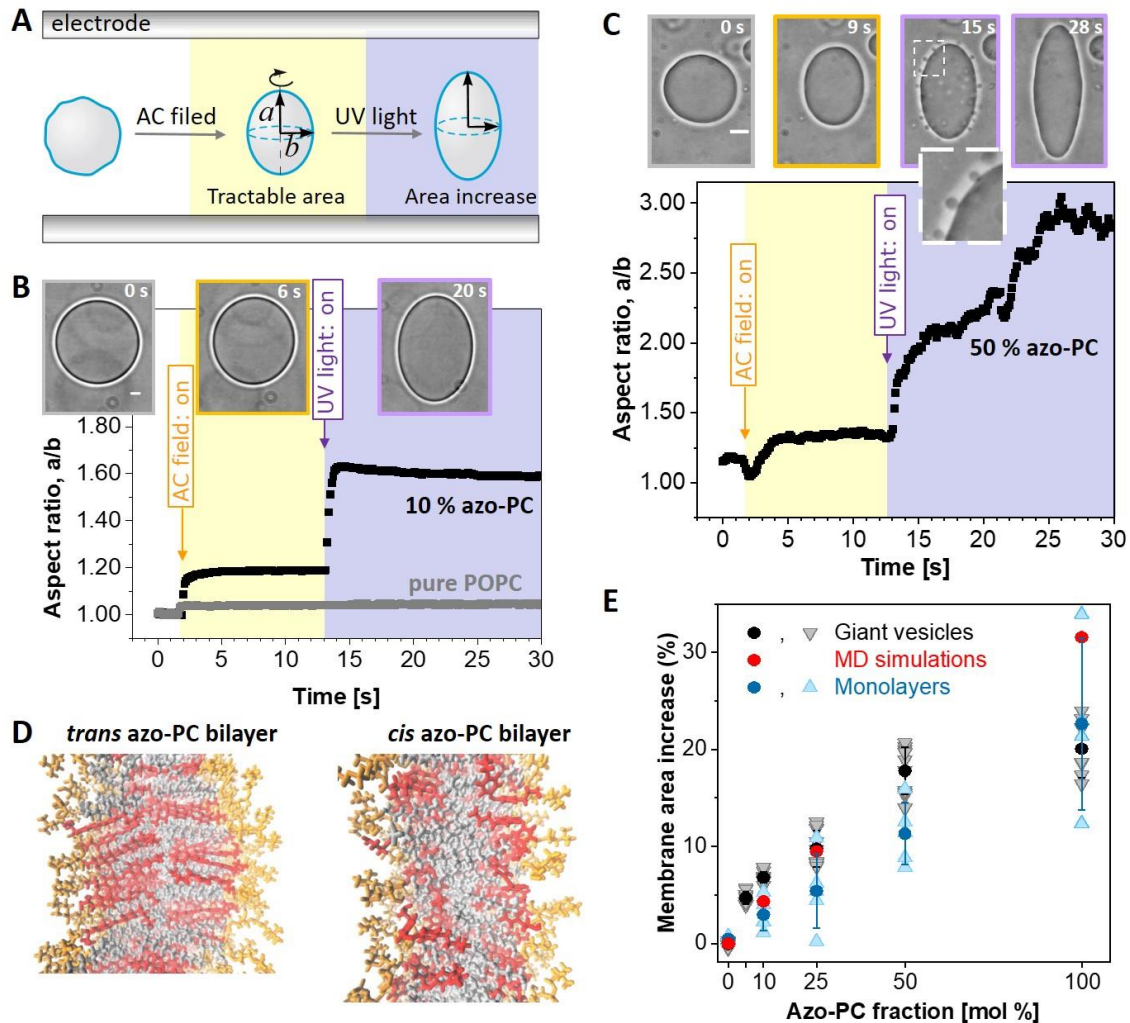


Figure 2: Area increase of membranes and monolayers doped with azo-PC when exposed to UV irradiation. (A) Sketch of the approach of GUV electrodeformation to assess the vesicle area change induced by UV light. The vesicles are first exposed to AC field (5 kV m^{-1} and 1 MHz) to pull out thermal fluctuations and deform them into a prolate ellipsoid with semi axes a and b . Then, while keeping the AC field on, the UV irradiation (365 nm) is initiated. (B, C) Electrodeformation and irradiation of GUVs made of pure POPC (gray trace in panel B) and containing 10 and 50 mol% azo-PC, see also Movies S4-S6 showing the response of these three vesicles. The snapshots show example images of the vesicles before applying the AC field (gray frame), after the application of AC field (orange frame) and when exposed to UV light (purple frame). A zoomed-up vesicle segment (dashed region) is given in C, showing the produced vesicle buds right after irradiation. The vesicle semi axes are used to calculate the vesicle area. (D) Snapshots from MD simulations bilayers composed of 100 mol% azo-PC in *trans* and *cis* conformation. The head groups of the lipids are in orange, the azo-benzene moiety in red, and the oleoyl tails in gray. The area of the bilayer increases and tith thickness decreases. (E) Membrane area expansion as assessed from GUV electrodeformation (gray symbols show data on individual GUVs; black data show mean and standard deviation, SD), MD simulations (red) Langmuir monolayer isotherms (light blue triangles show measurement of an individual Langmuir monolayers, dark blue – mean +/- SD).

The area increase of the cell mimetic vesicles resulting from azo-PC photoswitching was calculated from the ellipsoid surface area of the GUVs at their maximal deformation (Eq. 1) and by subtracting the initial electric field-driven deformation in the absence UV light. This subtraction eliminates effects associated with the initial membrane tension and the applied electric field. To account for the different vesicle sizes, we normalized the area by the initial one under electrodeformation in the dark. At least 10 vesicles per composition were examined. In the absence of azo-PC (pure POPC membranes), no

detectable change in the vesicle area due to UV light was observed suggesting that the illumination conditions (intensity and duration) do not alter the membrane. However, with raising the molar fraction of azo-PC lipids in the membrane, GUVs area increase could rise up to 20 % (gray and black data in Fig. 2E). Similar but smaller area change was found from dynamic light scattering (DLS) measurements on large unilamellar vesicles (LUVs, Fig. S3 and Methods section 2.7). It is worthwhile to note that the LUV hydrodynamic radius measured with DLS can be used to obtain only an apparent area change because an assumption for the vesicle shape (typically a sphere) is required. Thus, LUV measurements do not properly represent the vesicle area increase and lead to underestimates (Fig. S3). This emphasizes the superiority of our minimal cell model over LUVs for measuring area changes.

For higher fractions of azo-PC, the data on GUV area increase under UV exhibit larger scatter (larger standard deviations) and above 50 mol% azo-PC appear to reach saturation (Figs. 2E and S3). This is mostly due to the slow re-adsorption of the light-triggered buds as well as to the strongly elongated GUV shapes (observed for 100 mol% azo-PC) to which the elliptical approximation does not fully apply. Furthermore, the area of the photolipids is expected to be more packed and closely aligned at high azo-PC fractions, which could result in stronger dipole-dipole interactions between the azobenzenes in the lipid tails, potentially leading to photolipid clustering.^[30a, 54]

In order to test these hypotheses, find out whether they are universal and not constraint to our minimalistic model system, and to gain deeper insight at molecular level into this photoswitchable minimal cellular system, we performed MD simulations of membranes with azo-PC in *cis* and *trans* state (Fig. 2D). We also examined Langmuir monolayers with different compositions exposed to UV and blue light, respectively (Fig. S4). Both MD simulations and monolayer isotherms yield excellent agreement with the data from our minimal cell model showing relatively linear increase of the light-induced area change with increasing azo-PC fractions in the membrane (Fig. 2E). Even though linear, the expansion data of the monolayers lie somewhat lower compared to that from the bilayer systems (MD and GUV membranes). This is to be expected as the monolayer lacks all inter-leaflet interactions that are present in the bilayer (and discussed in more detail below) and faces air as less similar environment compared to that of the lipid chain moieties. The MD simulation, consistent with monolayer data, reveal that the area per lipid decreases with increasing fraction of *trans* azo-PC in the membrane and the opposite is true for the *cis* azo-PC conformation. The combined effect of these opposite trends yields an increase in the bilayer area by up to ~30 % for the pure azo-PC membrane (Fig. 2E). The quantitative match between the GUV model and MD simulations (except for the 100 mol% azo-PC case where the GUV electrodeformation approach lacks high accuracy) also suggests that under the selected irradiation conditions, full photoconversion of the azo-PC molecules occurs.

The simulations offer further insight in the origin of the membrane area changes as a function of photolipid fraction and isomerization state. The fairly rigid planar *trans* tails tend to orient along the membrane normal and can stack flatly against each other. The bent *cis* tails on the other hand orient more along the membrane plane and localize predominantly close to the headgroup-tail interface. As a result, the palmitoyl tails fill the region near the bilayer center, as clearly visible in the density profiles (Fig. S5).

3.3. Reversibility and kinetics of membrane response

To further examine the photoswitching efficiency on the bilayer, we investigated the reversibility and relaxation kinetics of the membrane response of azo-PC containing GUVs. Establishing a fully reversible and reproducible photoswitching process is an important criterion for the efficient regulation of membrane shape and mechanics. In order to fully reverse the photoswitching from *cis*-to-*trans* isomerization, we applied blue irradiation after exposing azo-PC GUVs to UV light. Upon reversible and complete photoswitching, the area expansion of the vesicle due to *trans*-to-*cis* isomerization under UV

light should be fully recovered and equal to the area shrinkage resulting from the *cis*-to-*trans* isomerization under the blue light. We compared the area changes under these two illumination conditions for GUVs containing 10 and 25 mol % azo-PC, where no complex budding events are observed and the area changes can be measured at high precision. The data are presented in Fig. 3A. Based on the results of the statistical tests, no significant differences were observed between the means of vesicle area changes for *trans*-to-*cis* and *cis*-to-*trans* isomerization for fixed membrane composition, indicating that light-induced morphological changes of azo-PC GUVs are reversible.

Similarly, the reversibility of swelling and shrinkage of GUVs due to photoswitching under UV and blue light were monitored several times (Fig. 3B, Movie S7). Vesicle deformation was fully reversible and could be switched back and forth over multiple cycles. Furthermore, we observed that the sharp contrast resulting from sugar asymmetry between GUV interior and exterior solutions was preserved, suggesting that during the multiple photoswitching cycles the membrane remains intact, i.e. the photoisomerization process did not generate any permeation or leakage over time. All these data illustrate that photoswitching under the selected irradiation conditions can be repeated without any sign of decomposition (of either azo-PC and POPC) or membrane leakage.

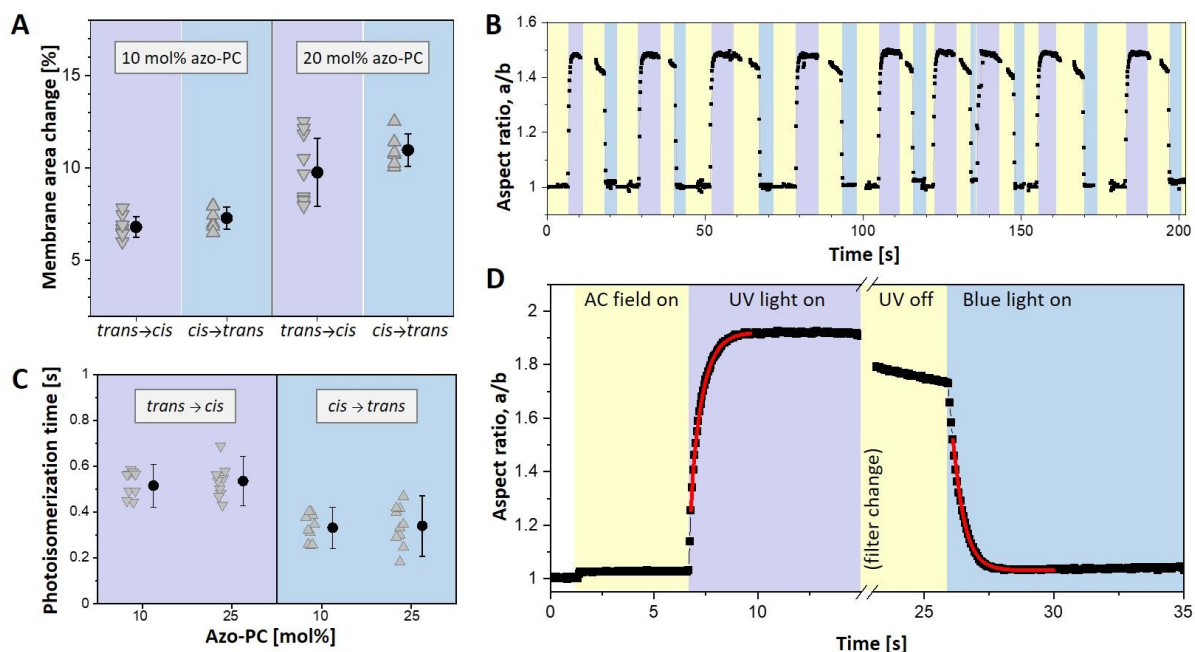


Figure 3: Photoswitching reversibility and kinetics assessed from the response of azo-PC GUVs exposed to UV and blue light. (A) Membrane area change measured on vesicles containing 10 and 25 mol % of azo-PC. *Trans*-to-*cis* isomerization upon UV illumination leads to area changes similar to that observed upon *cis*-to-*trans* isomerization under blue light. Each triangle indicates a measurement of an individual GUV. Mean and standard deviation values are also shown on the right. ANOVA test for null hypothesis testing for 10 and 25 mol % azo-PC GUVs gives respectively $p = 0.136$ and $p = 0.065$, indicating statistically insignificant difference for the *trans*-to-*cis* vs. *cis*-to-*trans* area change of membranes of a fixed fraction of azo-PC. (B) Multiple photoswitching cycles of 10 mol% azo-PC vesicle shown in terms of the degree of deformation (a/b , aspect ratio) under UV light (purple regions) and blue light (blue regions) sequentially switched on and off; the same vesicle is shown in Movie S7. Throughout the experiment, the GUV is continuously exposed to AC-field ($5 \text{ kV}\cdot\text{m}^{-1}$ and 1 MHz; yellow). Purple and blue regions in the graph schematically illustrate the time intervals when UV and blue light are switched on. (C) Photoisomerization kinetics of 10 and 25 mol % azo-PC containing GUVs. Data from individual GUVs are shown with triangles (10 vesicles per composition and condition were measured). Solid circles and line bars show means and standard deviations. (D) Kinetic trace of the aspect ratio response to UV and blue light irradiation of a GUV containing 25 mol% azo-PC. The exponential fits (red curves) yield the respective time constants as plotted in panel C. A short period of time is needed to mechanically change the filter at the microscope turret, during which the recording of the vesicle is paused.

Based on the area swelling and shrinkage of electrodeformed GUVs under UV and blue light, we assessed the rates of isomerization from the response of GUVs containing 10 and 25 mol % azo-PC over the course of photoswitching. An example kinetic trace and the rates of photoswitching obtained from exponential fits to the data for *trans*-to-*cis* and *cis*-to-*trans* isomerization are shown in Fig. 3C, D. Our results demonstrated that the *cis*-to-*trans* exponential time constant (with a mean value of 335 ms) is shorter than the *trans*-to-*cis* response time (525 ms). This faster *cis*-to-*trans* photoswitching kinetics is understandable considering that the *trans* isomer is thermodynamically more stable. We note that these rates depend not on the molecular isomerization kinetics which are in the femtosecond to picosecond time range^[55] but is determined by the vesicle hydrodynamics and membrane viscosity. Photoisomerization kinetics did not show any difference between 10 to 25 mol % azo-PC containing vesicles.

3.4. Membrane mechanics

Considering the differences detected in the bilayer area, structure, and photoisomerization kinetics of *cis* and *trans* azo-PC GUVs, we hypothesized that membrane mechanical properties should also show differences depending on isomerization state and photoswitch fraction. Previous studies have already reported changes in bending rigidity as a function of photoswitch conformation in pure azo-PC membranes^[29] and have shown membrane softening with increasing azo-PC fractions in vesicles made of the synthetic diphytanoyl lipid (DPhPC)^[30a] (here we explore the effects in membranes of POPC – a naturally occurring lipid). These earlier studies employed micropipette aspiration and optical trapping in flow to assess the bending rigidity. Both of these approaches rely on mechanical deformation of the membrane, and it is well known, that such techniques can suffer from stretching contributions^[56]. Here, we employed fluctuation spectroscopy^[32, 35, 57] as a contactless approach to characterize the bending rigidity of POPC membranes with various fractions of azo-PC in different isomerization states (Fig. S6A). In parallel, computational studies have been performed to calculate the bending rigidity of the simulated membranes from the real space fluctuations of the tilt and splay of lipid tails^[49]. The absolute values obtained from experiment and simulations are expected to differ (as we find, see Fig. S6B), because the bending rigidity is sensitive to the composition of solutes in the bathing medium^[56] (pure water in simulations and sugar solutions in the experiment). To allow comparison, the results were normalized by the mean value of the bending rigidity measured for pure POPC membranes, Fig. 4A.

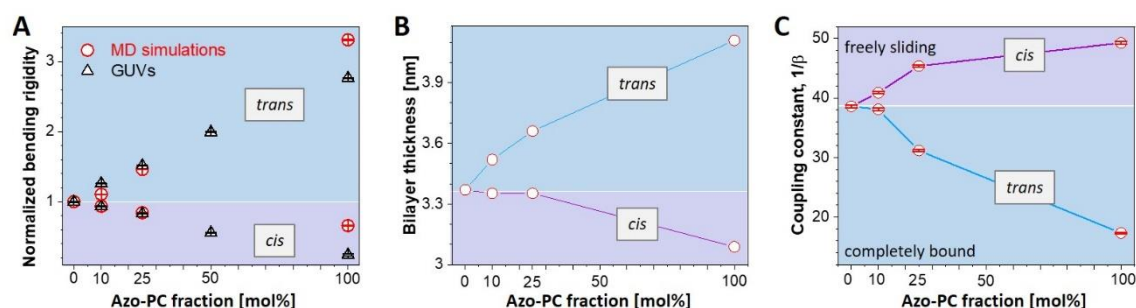


Figure 4: Bending rigidity, thickness and interleaflet coupling in membranes with various fractions of azo-PC in the *cis* and *trans* states. (A) Bending rigidity obtained from fluctuation spectroscopy (open triangles) and MD simulations (open circles). The results are normalized by the bending rigidity value of pure POPC (see non-normalized data in Figure S6). Blue and purple data correspond to *trans* and *cis* azo-PC, respectively. For each composition 10 GUVs are analyzed. Standard deviations are illustrated with line bars, smaller than the sizes of the symbols. (B) Bilayer thickness data at various fraction of azo-PC in *trans* and *cis* conformation obtained from

MD simulations. (C) Interleaflet coupling in *cis* and *trans* azo-PC containing bilayers. The coupling constant is deduced from simulation data by using the formula based on polymer brush model^[58], in which the elasticity ratio scales quadratically with hydrophobic thickness of the bilayer ($\kappa/K = \beta d^2$) and $1/\beta$ describes the coupling between the bilayer leaflets. Purple and blue trends demonstrate the coupling constants for *cis* and *trans* bilayers, respectively. Line bars are standard deviations and smaller than the size of the symbols.

We find excellent agreement between experiment and simulations demonstrating adeptness of the used force fields. Membranes doped with azo-PC in the *cis* conformation have lower bending rigidity compared to pure POPC and *trans* azo-PC GUVs, therefore, *cis*-photoisomerization of azo-PC softens the membrane. On the one hand, as the *cis* azo-PC fraction in the membrane increased from 0 to 100 mol%, the bending rigidity decreased 4 fold dropping down to values as low as 5 k_BT (Fig. S6A); similar bending rigidity decrease has been observed upon the insertion of fusion peptides^[59] pointing to the destabilizing potential of azo-PC. On the other hand, equivalently increasing *trans* azo-PC fractions in the membrane stiffens the membrane 3 fold reaching bending rigidity values around 70 k_BT (Figs. 4A and S6A); such bending rigidities are characteristic of membranes in the liquid ordered phase^[35, 60]. This is indeed consistent with the strong alignment of the azo-PC tails structurally resembling liquid ordered phases.

A simplistic reason for the changes in the bending rigidity could be sought in changes in the membrane thickness due to photoisomerization. X-ray scattering studies on pure azo-PC vesicles have shown thinning of the bilayer by approximately 4-5 Å resulting from *trans*-to-*cis* isomerization^[61]. Thinner membranes are generally softer and *vice versa*. We thus explored how the membrane thickness varies with azo-PC fraction and isomerization. MD simulations show that isomerization and increasing azo-PC fractions can alter membrane thickness by almost 1 nm (Fig. 4B). Membranes containing azo-PC in the *trans* state are more influenced by the photolipid fraction. The strong light-induced change in membrane thickness offers convenient means to manipulate and modulate the functionality of transmembrane proteins.

In addition to thickness changes as a reason for softening the membrane, the bending rigidity behavior in Fig. 4A could also be related to dipole-dipole coupling between azobenzene groups in the acyl chains of the photolipids.^[30a, 54] Stronger molecular interactions between photolipids might lead to more densely packed bilayer giving less flexibility to the membrane for bending. Another factor modulating the membrane mechanics is the interleaflet coupling, which relates the bending rigidity, κ , the stretching elasticity, K , and the membrane thickness, d . The relation of the two elastic moduli κ and K has been theoretically considered^[58, 62] and experimentally explored for pure lipid membranes^[62a]. Their ratio scales quadratically with the membrane thickness: $\kappa/K = \beta d^2$, where the proportionality constant β described the coupling of the monolayers constituting the membrane. For $1/\beta = 12$, the leaflets are completely bound^[62a], for $1/\beta = 48$, they are unbound and freely sliding^[62b], while the polymer brush model^[58] predicts the intermediate value of $1/\beta = 24$ for lipid bilayers. To resolve the leaflet coupling in our azo-PC membranes, we first assessed the stretching elasticity modulus K from MD simulations. This was achieved from fitting the tension versus area curves (see Methods section 2.6), which did not show any systematic dependence on azo-PC fraction in the bilayer. A combined fit to all data points resulted in a value of $K = 221.8 \pm 6.8$ mN/m which we kept constant for all calculations. The coupling constant values were then estimated for the corresponding fractions of *cis* and *trans* azo-PC in the bilayer using the simulation data for the bending rigidity and the membrane thickness, see Fig. 4C. Increasing the *trans* azo-PC fraction in the membrane from 0 to 100 mol % causes a decrease in $1/\beta$ from 35.6 ± 0.2 to 17.3 ± 0.1 . These results indicate stronger interleaflet interactions in the *trans* azo-PC bilayer. The opposite is true for increasing fractions of *cis*-azo-PC, which result in $1/\beta$ values corresponding to freely sliding monolayers, i.e., interleaflet interactions become weaker.

All these results clearly demonstrate that membrane elasticity of azo-PC vesicles and monolayer interactions can be conveniently regulated by light.

3.5. Photoresponse of minimal cells to exogenous addition of azo-PC

Above we provided a detailed characterization of photo-triggered membrane remodeling events on vesicle bilayers prepared from POPC and varying fractions of azo-PC. In view of the potential application of the photoswitch to modulating the mechanics, area, and morphology of cellular membranes, we raise the question whether it is possible to observe similar membrane dynamics and photoresponse upon incubating pure POPC membranes in solutions containing the azo-PC photoswitch. Such exogenous incorporation of azo-PC into the already established membrane bilayers is a prerequisite for the direct manipulation of cells. We hypothesized that the amphiphilic nature of azo-PC molecule may enable the membrane to adsorb this photoswitch from the external media to the outer leaflet of the bilayer asymmetrically thus rendering the membrane photoresponsive.

POPC GUVs were prepared and incubated in a solution of azo-PC at a concentration equal to that of the total lipid concentration in the GUV suspension, see Methods section 2.8. In this way, we aimed at obtaining vesicles with 50 mol% azo-PC. After 20 min incubation in the azo-PC solution, and prior to UV illumination, most GUVs appeared tubulated (see first snapshot in Fig. 5A). Controls based on the addition of the same amounts of azo-PC-free solution resulted in no detectable changes in the GUV morphology. Asymmetric distribution of amphiphilic molecules in the membrane is known to induce membrane tubulation stabilized by spontaneous curvature^[63]. The outward formation of tubes of micron-sized diameters that we observe indicates that the final distribution of azo-PC in the bilayer is only slightly asymmetric resulting in small positive spontaneous curvature. Presumably, the incorporation of photolipid is associated with lipid flip-flop to compensate the large area increase of the vesicle outer leaflet upon the incorporation of 50 mol% azo-PC.

Upon UV illumination, quasi-spherical GUVs with a few outer tubes transform into tubular networks or highly tubulated morphologies. This process occurs within a couple of seconds of irradiation (see Movie S8). The protrusions retract back under blue light (Fig. 5). These morphological transformations could be reversed back and forth over multiple photoswitching cycle (Fig. 5A). This result demonstrates the reversibility of the light-induced manipulation of exogenously doped azo-PC vesicles. Thus, we conclude that light-triggered membrane remodeling events on cells exogenously exposed to azo-PC is feasible.

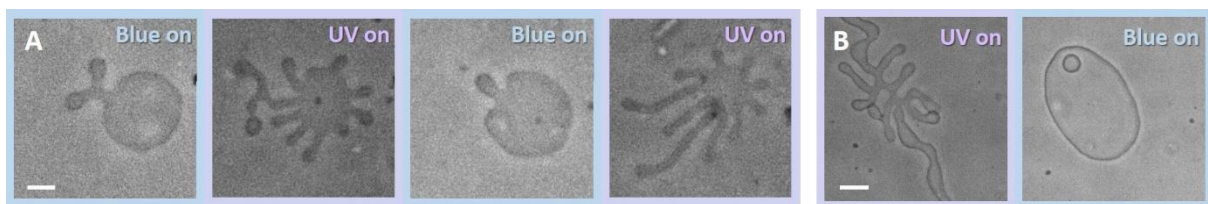


Figure 5: Two examples of the photoresponse of POPC vesicles exogenously doped with azo-PC and irradiated with UV and blue light. The vesicles were exposed to a solution of azo-PC at 15.56 μM bulk concentration (equivalent to the total lipid concentration in the GUV suspension). The GUVs adopt highly tubulated morphologies under the exposure of UV light (365 nm). Under blue light irradiation (450 nm), most of the tubules are re-adsorbed and the vesicles adopt their initial non-tubulated morphology, see also Movie S8. Illumination conditions are indicated on upper-right side of each snapshot. The scale bars correspond to 10 μm .

4. Conclusions

In summary, we employ light as a facile, fast and sustainable tool for micromanipulation of artificial minimal cells in combination with the photoswitch azo-PC as a converter of light to mechanical energy.

By using a comprehensive set of experimental and computational approaches, we have constructed a holistic description of the membrane response to photoisomerization in terms of membrane expansion, thinning, and softening. We also demonstrate the biomimetic potential of the photo-triggered biomachinery to modulate shape-dependent cellular processes such as endo/exocytosis and intra/intercellular trafficking. Photoisomerization of azo-PC under UV-A and blue light triggers complex shape transformations and budding events in the membrane, which could be finely tuned by altering the molar fraction of azo-PC in the membrane. The potential phototoxicity of UV and blue light can be remedied by shifting the excitation wavelength of azobenzene derivatives into the lower energy range as recently demonstrated^[64]. The reversibility of the photoisomerization process provides us with high temporal control and accuracy for multiple cycles of photoswitching. Our studies with GUVs, LUVs, Langmuir monolayers and MD simulations consistently illustrate that light-induced membrane deformations due to photoisomerization of azo-PC cause dynamic changes in bilayer packing, membrane elasticity as well as interleaflet interactions thus leading to dramatic changes in the material properties of cell membranes, which scale with azo-PC fraction. Light-triggered morphology responses are reproducible even upon exogenous insertion of azo-PC in the membrane of already formed vesicles, which provides a promising background for intercalating this photoswitch in more complex cell systems to optically control the cellular activities.

Author contributions

MA performed all vesicle-based work. AG performed the simulations. FC performed the experiments on monolayers. MA, VG, FC, AG analyzed data. RD and JH proposed the project. RD supervised the project. MA and RD wrote the manuscript with contributions from all authors.

Declaration of interests

The authors declare no competing interests.

Acknowledgements

MA acknowledges funding from the International Max Planck Research School on Multiscale BioSystems. This work was supported by Germany's Excellence Strategy, EXC 2008/1 (UniSysCat), Grant 390540038.

References

- [1] a)S. Masiero, S. Lena, S. Pieraccini, G. P. Spada, *Angewandte Chemie International Edition* **2008**, 47, 3184; b)Z. Wang, P. Erhart, T. Li, Z.-Y. Zhang, D. Sampedro, Z. Hu, H. A. Wegner, O. Brummel, J. Libuda, M. B. Nielsen, K. Moth-Poulsen, *Joule* **2021**, 5, 3116.
- [2] a)F. Höglspenger, T. Betz, B. J. Ravoo, *ACS Macro Letters* **2022**, 11, 537; b)J. Boelke, S. Hecht, *Advanced Optical Materials* **2019**, 7, 1900404.
- [3] P. Klán, J. Wirz, in *Molecular Photoswitches*, 2022.
- [4] a)H. A. Wegner, *Angewandte Chemie International Edition* **2012**, 51, 2281; b)V. Balzani, M. Clemente-León, A. Credi, B. Ferrer, M. Venturi, A. H. Flood, J. F. Stoddart, *Proc Natl Acad Sci U S A* **2006**, 103, 1178; c)N. Katsonis, M. Lubomska, M. M. Pollard, B. L. Feringa, P. Rudolf, *Progress in Surface Science* **2007**, 82, 407.
- [5] a)H. M. D. Bandara, S. C. Burdette, *Chemical Society Reviews* **2012**, 41, 1809; b)A. A. Beharry, G. A. Woolley, *Chem. Soc. Rev.* **2011**, 40, 4422.
- [6] L. Dong, Y. Feng, L. Wang, W. Feng, *Chemical Society Reviews* **2018**, 47, 7339.

- [7] R. S. Stoll, M. V. Peters, A. Kuhn, S. Heiles, R. Goddard, M. Bühl, C. M. Thiele, S. Hecht, *Journal of the American Chemical Society* **2009**, 131, 357.
- [8] A. Kopyshev, K. Kanevche, N. Lomadze, E. Pfitzner, S. Loebner, R. R. Patil, J. Genzer, J. Heberle, S. Santer, *ACS Applied Polymer Materials* **2019**, 1, 3017.
- [9] a)I. A. Banerjee, L. Yu, H. Matsui, *Journal of the American Chemical Society* **2003**, 125, 9542; b)M. Liu, X. Yan, M. Hu, X. Chen, M. Zhang, B. Zheng, X. Hu, S. Shao, F. Huang, *Organic Letters* **2010**, 12, 2558.
- [10] P. Leippe, J. A. Frank, *Current Opinion in Structural Biology* **2019**, 57, 23.
- [11] H. Nakano, T. Takahashi, T. Kadota, Y. Shirota, *Advanced Materials* **2002**, 14, 1157.
- [12] a)J. Liu, W. Bu, L. Pan, J. Shi, *Angewandte Chemie International Edition* **2013**, 52, 4375; b)W. A. Velema, W. Szymanski, B. L. Feringa, *Journal of the American Chemical Society* **2014**, 136, 2178; c)N. Chander, J. Morstein, J. S. Bolten, A. Shemet, P. R. Cullis, D. Trauner, D. Witzigmann, *Small* **2021**, 17, 2008198.
- [13] J. Morstein, D. Trauner, *Current Opinion in Chemical Biology* **2019**, 50, 145.
- [14] a)S. Kellner, S. Berlin, *Applied Sciences* **2020**, 10, 805; b)K. Hüll, J. Morstein, D. Trauner, *Chemical Reviews* **2018**, 118, 10710.
- [15] N. Tamai, H. Miyasaka, *Chem Rev* **2000**, 100, 1875.
- [16] A. Yoshida, N. Sakai, Y. Uekusa, Y. Imaoka, Y. Itagaki, Y. Suzuki, S. H. Yoshimura, *PLoS Biol* **2018**, 16, e2004786.
- [17] F. L. Urbina, S. M. Gomez, S. L. Gupton, *Journal of Cell Biology* **2018**, 217, 1113.
- [18] a)S. Maharana, K. V. Iyer, N. Jain, M. Nagarajan, Y. Wang, G. V. Shivashankar, *Nucleic Acids Res* **2016**, 44, 5148; b)C. Cadart, E. Zlotek-Zlotkiewicz, M. Le Berre, M. Piel, Helen K. Matthews, *Developmental Cell* **2014**, 29, 159.
- [19] S. B. Khatau, S. Kusuma, D. Hanjaya-Putra, P. Mali, L. Cheng, J. S. Lee, S. Gerecht, D. Wirtz, *PLoS One* **2012**, 7, e36689.
- [20] J. Tong, Y. Qi, X. Wang, L. Yu, C. Su, W. Xie, J. Zhang, *Biochim Biophys Acta Mol Cell Res* **2017**, 1864, 2389.
- [21] J. V. Shah, *J Cell Biol* **2010**, 191, 233.
- [22] F. L. Au - Kriegel, R. Au - Köhler, J. Au - Bayat-Sarmadi, S. Au - Bayerl, A. E. Au - Hauser, R. Au - Niesner, A. Au - Luch, Z. Au - Cseresnyes, *JoVE* **2018**, e58543.
- [23] a)P. Pascual-Vargas, S. Cooper, J. Sero, V. Bousgouni, M. Arias-Garcia, C. Bakal, *Scientific Data* **2017**, 4, 170018; b)S. M. Lyons, E. Alizadeh, J. Mannheimer, K. Schuamberg, J. Castle, B. Schroder, P. Turk, D. Thamm, A. Prasad, *Biol Open* **2016**, 5, 289; c)A. Pasqualato, A. Palombo, A. Cucina, M. A. Mariggiò, L. Galli, D. Passaro, S. Dinicola, S. Proietti, F. D'Anselmi, P. Coluccia, M. Bizzarri, *Exp Cell Res* **2012**, 318, 835.
- [24] a)A. Saraste, K. Pulkki, *Cardiovasc Res* **2000**, 45, 528; b)G. Häcker, *Cell Tissue Res* **2000**, 301, 5; c)U. Ziegler, P. Groscurth, *Physiology* **2004**, 19, 124.
- [25] a)R. Dimova, *Annu. Rev. Biophys.* **2019**, 48, 93; b)R. Dimova, C. Marques, *The Giant Vesicle Book*, Taylor & Francis Group, LLC, Boca Raton **2019**.
- [26] J. B. Manneville, P. Bassereau, D. Levy, J. Prost, *Phys. Rev. Lett.* **1999**, 82, 4356.
- [27] a)H. Erkan-Candag, D. Krivic, M. A. F. Gsell, M. Aleksanyan, T. Stockner, R. Dimova, O. Tiapko, K. Groschner, *Biomolecules*, 10.3390/biom12060799; b)J. Pfeffermann, B. Eicher, D. Boytsov, C. Hanneschlaeger, T. R. Galimzyanov, T. N. Glasnov, G. Pabst, S. A. Akimov, P. Pohl, *J. Photochem. Photobiol. B: Biol.* **2021**, 224, 112320; c)V. N. Georgiev, A. Grafmüller, D. Bléger, S. Hecht, S. Kunstmann, S. Barbirz, R. Lipowsky, R. Dimova, *Advanced Science* **2018**, 5, 1800432; d)A. Diguët, M. Yanagisawa, Y.-J. Liu, E. Brun, S. Abadie, S. Rudiuk, D. Baigl, *Journal of the American Chemical Society* **2012**, 134, 4898; e)F. Crea, A. Vorkas, A. Redlich, R. Cruz, C. Shi, D. Trauner, A. Lange, R. Schlesinger, J. Heberle, *Frontiers in Molecular Biosciences* **2022**, 9.
- [28] a)E. Karatekin, O. Sandre, H. Guitouni, N. Borghi, P. H. Puech, F. Brochard-Wyart, *Biophys. J.* **2003**, 84, 1734; b)O. Sandre, L. Moreaux, F. Brochard-Wyart, *Proc. Natl. Acad. Sci. U. S. A.* **1999**, 96, 10591.

- [29] C. Pernpeintner, J. A. Frank, P. Urban, C. R. Roeske, S. D. Pritzl, D. Trauner, T. Lohmüller, *Langmuir* **2017**, 33, 4083.
- [30] a)P. Urban, S. D. Pritzl, D. B. Konrad, J. A. Frank, C. Pernpeintner, C. R. Roeske, D. Trauner, T. Lohmüller, *Langmuir* **2018**, 34, 13368; b)S. D. Pritzl, P. Urban, A. Prasselsperger, D. B. Konrad, J. A. Frank, D. Trauner, T. Lohmüller, *Langmuir* **2020**, 36, 13509.
- [31] S. Aranda, K. A. Riske, R. Lipowsky, R. Dimova, *Biophys. J.* **2008**, 95, L19.
- [32] H. A. Faizi, C. J. Reeves, V. N. Georgiev, P. M. Vlahovska, R. Dimova, *Soft Matter* **2020**, 16, 8996.
- [33] a)K. A. Riske, T. P. Sudbrack, N. L. Archilha, A. F. Uchoa, A. P. Schroder, C. M. Marques, M. S. Baptista, R. Itri, *Biophysical Journal* **2009**, 97, 1362; b)R. B. Lira, T. Robinson, R. Dimova, K. A. Riske, *Biophys. J.* **2019**, 116, 79.
- [34] a)R. Dimova, K. A. Riske, in *Handbook of Electroporation*, (Ed: D. Miklavčič), Springer International Publishing, Cham 2017; b)M. Aleksanyan, H. A. Faizi, M.-A. Kimpaki, P. M. Vlahovska, K. A. Riske, R. Dimova, *Advances in Physics: X* **2023**, 8, 2125342.
- [35] R. S. Gracià, N. Bezlyepkina, R. L. Knorr, R. Lipowsky, R. Dimova, *Soft Matter* **2010**, 6, 1472.
- [36] C. J. Dickson, B. D. Madej, Å. A. Skjevik, R. M. Betz, K. Teigen, I. R. Gould, R. C. Walker, *Journal of Chemical Theory and Computation* **2014**, 10, 865.
- [37] P. Duchstein, C. Neiss, A. Görling, D. Zahn, *Journal of Molecular Modeling* **2012**, 18, 2479.
- [38] J. Wang, R. M. Wolf, J. W. Caldwell, P. A. Kollman, D. A. Case, *Journal of computational chemistry* **2004**, 25, 1157.
- [39] F. Y. Dupradeau, A. Pigache, T. Zaffran, C. Savineau, R. Lelong, N. Grivel, D. Lelong, W. Rosanski, P. Cieplak, *Phys Chem Chem Phys* **2010**, 12, 7821.
- [40] M. Wehle, I. Vilotijevic, R. Lipowsky, P. H. Seeberger, D. Varon Silva, M. Santer, *Journal of the American Chemical Society* **2012**, 134, 18964.
- [41] a)S. Jo, T. Kim, V. G. Iyer, W. Im, *Journal of Computational Chemistry* **2008**, 29, 1859; b)S. Jo, J. B. Lim, J. B. Klauda, W. Im, *Biophysical Journal* **2009**, 97, 50; c)E. L. Wu, X. Cheng, S. Jo, H. Rui, K. C. Song, E. M. Dávila-Contreras, Y. Qi, J. Lee, V. Monje-Galvan, R. M. Venable, J. B. Klauda, W. Im, *Journal of Computational Chemistry* **2014**, 35, 1997.
- [42] D. Case, T. Darden, T. Cheatham III, C. Simmerling, J. Wang, R. Duke, R. Luo, R. Walker, W. Zhang, K. Merz, *Google Scholar There is no corresponding record for this reference*.
- [43] W. Humphrey, A. Dalke, K. Schulten, *Journal of molecular graphics* **1996**, 14, 33.
- [44] W. L. Jorgensen, J. Chandrasekhar, J. D. Madura, R. W. Impey, M. L. Klein, *The Journal of Chemical Physics* **1983**, 79, 926.
- [45] a)M. J. Abraham, T. Murtola, R. Schulz, S. Páll, J. C. Smith, B. Hess, E. Lindahl, *SoftwareX* **2015**, 1-2, 19; b)D. Van Der Spoel, E. Lindahl, B. Hess, G. Groenhof, A. E. Mark, H. J. C. Berendsen, *Journal of computational chemistry* **2005**, 26, 1701.
- [46] H. J. Berendsen, J. v. Postma, W. F. van Gunsteren, A. DiNola, J. R. Haak, *The Journal of chemical physics* **1984**, 81, 3684.
- [47] a)S. Nosé, *Molecular physics* **1984**, 52, 255; b)W. G. Hoover, *Physical review A* **1985**, 31, 1695.
- [48] a)M. Parrinello, A. Rahman, *Journal of Applied physics* **1981**, 52, 7182; b)S. Nosé, M. L. Klein, *Molecular Physics* **1983**, 50, 1055.
- [49] M. Doktorova, D. Harries, G. Khelashvili, *Physical Chemistry Chemical Physics* **2017**, 19, 16806.
- [50] N. Johnner, D. Harries, G. Khelashvili, *BMC Bioinformatics* **2016**, 17, 161.
- [51] H. Bouvrais, T. Pott, L. A. Bagatolli, J. H. Ipsen, P. Meleard, *Biochim. Biophys. Acta-Biomembr.* **2010**, 1798, 1333.
- [52] N. F. Morales-Pennington, J. Wu, E. R. Farkas, S. L. Goh, T. M. Konyakhina, J. Y. Zheng, W. W. Webb, G. W. Feigenson, *Biochim. Biophys. Acta* **2010**, 1798, 1324.
- [53] H. A. Faizi, R. Dimova, P. M. Vlahovska, *Biophys. J.* **2022**, 121, 910.
- [54] a)V. Czikkely, H. D. Forsterling, H. Kuhn, *Chemical Physics Letters* **1970**, 6, 207; b)A. Einfeld, J. S. Briggs, *Chemical Physics* **2006**, 324, 376.
- [55] T. Nägele, R. Hoche, W. Zinth, J. Wachtveitl, *Chem. Phys. Lett.* **1997**, 272, 489.
- [56] R. Dimova, *Adv. Colloid Interface Sci.* **2014**, 208, 225.
- [57] H. A. Faizi, S. L. Frey, J. Steinkühler, R. Dimova, P. M. Vlahovska, *Soft Matter* **2019**, 15, 6006.

- [58] E. A. Evans, *Biophysical Journal* **1974**, 14, 923.
- [59] a)P. Shchelokovskyy, S. Tristram-Nagle, R. Dimova, *New J. Phys.* **2011**, 13, 025004; b)S. Tristram-Nagle, R. Chan, E. Kooijman, P. Uppamoochikkal, W. Qiang, D. P. Weliky, J. F. Nagle, *Journal of Molecular Biology* **2010**, 402, 139.
- [60] A. W. Tian, B. R. Capraro, C. Esposito, T. Baumgart, *Biophys. J.* **2009**, 97, 1636.
- [61] P. Urban, S. D. Pritzl, M. F. Ober, C. F. Dirscherl, C. Pernpeintner, D. B. Konrad, J. A. Frank, D. Trauner, B. Nickel, T. Lohmueller, *Langmuir* **2020**, 36, 2629.
- [62] a)W. Rawicz, K. C. Olbrich, T. McIntosh, D. Needham, E. Evans, *Biophys J* **2000**, 79, 328; b)R. Goetz, G. Gompper, R. Lipowsky, *Physical Review Letters* **1999**, 82, 221.
- [63] a)R. Dasgupta, M. S. Miettinen, N. Fricke, R. Lipowsky, R. Dimova, *Proceedings of the National Academy of Sciences* **2018**, 115, 5756; b)M. Aleksanyan, R. B. Lira, J. Steinkühler, R. Dimova, *Biophys. J.* **2022**, 121, 3295; c)S. A. Gandhi, C. V. Kelly, *Biophysical Journal* **2022**, 121, 3173; d)P. Bassereau, R. Jin, T. Baumgart, M. Deserno, R. Dimova, V. A. Frolov, P. V. Bashkirov, H. Grubmüller, R. Jahn, H. J. Risselada, L. Johannes, M. M. Kozlov, R. Lipowsky, T. J. Pucadyil, W. F. Zeno, J. C. Stachowiak, D. Stamou, A. Breuer, L. Lauritsen, C. Simon, C. Sykes, G. A. Voth, T. R. Weikl, *J. Phys. D: Appl. Phys.* **2018**, 51, 343001.
- [64] S. D. Pritzl, D. B. Konrad, M. F. Ober, A. F. Richter, J. A. Frank, B. Nickel, D. Trauner, T. Lohmüller, *Langmuir* **2022**, 38, 385.